Co-sensitized dye-sensitized solar cells based on d^{10} coordinate complexes towards their optoelectronic properties†

Xin Wang, Yulin Yang,* Ruiqing Fan* and Zhaohua Jiang

Received (in Gainesville, FL, USA) 18th April 2010, Accepted 11th June 2010
DOI: 10.1039/c0nj00361a

Three five-coordinate transition metal complexes [2,6-$(PhN{=}CMe)_2C_5H_3NMCl_2{\cdot}CH_3CN$] (M = Zn, Cd, Hg) (named **M1**) have been assembled onto a nanocrystalline TiO_2 film to prepare transition metal complex/N719 co-sensitized photoelectrodes for dye-sensitized solar cell applications. The metal center is chelated in a tridentate manner by the ligand and further coordinated by two chlorine atoms, resulting in distorted trigonal bipyramidal geometry. In the tandem structure of the TiO_2/**M1**/dye electrode, the **M1** undergoes a re-organization of energy levels due to its single-crystal structure, which is advantageous to electron injection and hole recovery. The co-sensitized structure is proved to have a superior ability, when compared to a single N719 dye's influence on TiO_2. Therefore, co-sensitized solar cells based on TiO_2/**M1**/N719 electrodes yield a remarkably high photocurrent density (J_{sc}), open circuit voltage (V_{oc}) and energy conversion efficiency under standard global AM1.5 solar irradiation conditions, which are relatively higher than those for DSSCs using single organic sensitizers.

Introduction

Conversion of solar energy into electrical energy using photovoltaic cells (PVC) is arguably one of the most successful and environmentally friendly technologies for energy generation.[1,2] In the original dye-sensitized solar cell (DSSC) developed in 1991 by O'Regan and Grätzel,[3] TiO_2 nanoparticle films were sensitized with N3 (Ruthenium organic dye) of high cost.[4] Recently, efforts for increasing solar cell efficiency while maintaining a low production cost have been the primary objective of solar energy conversion, such as the use of combining QD sensitization, polymers and other cheap metal–organic complexes as sensitizers in TiO_2 nanoparticle solar cells.[5–7] Metal coordination organic dyes have been used and applied in DSSCs to assess the current status in research and future developments in a broad and rapidly growing area of technology due to their low cost of production.[8–10] Organic dyes offer infinite possibilities for improving a wide range of properties, such as molecular structure and function, efficient light-harvesting ability in different parts of the solar spectrum, control over the molecular energy levels, charge generation and separation, and molecule-to-molecule interactions. The major advantage of organic materials for solar cell applications is that they can function both as a hole transporter as well as a sensitizer for such nanocrystalline solar cells. They are easy to design with a very high light absorbing capacity. meaning that thinner films can be used to generate optimal photovoltaic performance. Although remarkable advances have been made with metal coordination organic dyes as sensitizers in DSSCs, there is still a need to optimize their chemical and physical properties to further improve solar cells. An appropriate sensitizer for DSSCs should have an inverted arrangement of the donor and acceptor moieties in the dye molecule for efficient hole injection into the photocathode. A way to improve efficiency is by the co-adsorption of dyes with additives and by structural modifications with bulky substituents that can prevent p–p stacking or dye aggregation.[11–13] The co-sensitization approach is also very appealing for using multiple dyes to obtain panchromatic absorption, but the fine-tuning seems to be quite difficult. Ehret *et al.* studied a nanocrystalline TiO_2 solar cell sensitized by various dicarboxylated cyanines and found that the use of mixed cyanine dyes could improve photoelectric conversion efficiency.[14] Zhang and co-workers examined the mechanism of co-sensitization with squarylium and N3 dyes by time-resolved spectroscopy.[15] Guo *et al.* studied the co-sensitization of cyanine dyes. A combination of the two dyes in a 1 : 3 ratio was found to cover the entire visible spectrum, thereby generating a conversion yield of 3.4%, which is higher than that of the TiO_2 electrode sensitized with a single dye.[16] A combination of three dyes, such as 4-dimethylaminophenyl-cyanoacrylic acid, which absorb in the yellow (380 nm), red (535 nm) and blue (642 nm) regions, respectively, were employed as co-sensitizers in liquid DSSCs. Recently, Grätzel and co-workers combined bisthiophene dye JK2 with squarylium cyanine dye SQ1 as co-sensitizers and obtained an overall conversion efficiency of 7.43%.[17] This value is so far the highest value reported for co-sensitized DSSCs with metal coordination organic dyes. Herein, the research selects three [bis(iminoalkyl)pyridine] ligand complexes we have previously reported as co-sensitized photoelectrodes for a study of their photoelectrochemical properties in DSSCs. It also discusses the relationships between molecule structure and electrochemistry properties. Worth mentioning here is that this research represents the first example where 2,6-bis(imino)pyridyl-type inorganic coordinate complexes are co-sensitized with N719 in TiO_2, forming composite photoelectrodes. Undoubtedly, they play

Department of Applied Chemistry, Harbin Institute of Technology, Harbin, 150001, P. R. China. E-mail: ylyang@hit.edu.cn, fanruiqing@hit.edu.cn

† Electronic supplementary information (ESI) available: Further experimental data. See DOI: 10.1039/c0nj00361a

an important role in optimization matching with dyes of electricity conversion efficiencies in compounds.

Experimental section

Synthesis of transition metal complexes

The pyridine-2,6-dicarboxylic acid was prepared by oxidation reaction from 2,6-dimethylpyridine. 2,6-Dimethylpyridine (20 mL, 0.17 mol) was added to 500 mL water, potassium permanganate (54.4 g, 0.34 mol) slowly added and the mixture then heating until the disappearance of the purple colour. Another portion of potassium permanganate (54.4 g, 0.34 mol) and water (300 mL) was then slowly added and the mixture heated. After 2–3 h, the purple color disappeared again and the reaction was cooled to room temperature. Filtration and removal of the solvent was undertaken until the residual volume was down to 200 mL. Then, sulfuric acid (70%, 35 mL) was added slowly and the precipitate filtered to afford pyridine-2,6-dicarboxylic acid as a white solid (20.62 g, yield: 71.8%).

2,6-Bis[1-(2,6-dimethylphenylimino)ethyl]pyridine ($\mathbf{L^2}$) was synthesized according to modified published procedures in good yield by condensation of 2,6-diacetylpyridine with the corresponding aniline in refluxing absolute methanol in the presence of a catalytic amount of formic acid (Scheme 1).

Zn1 ($C_{33}H_{43}N_3ZnCl_2$). Zinc complexes were synthesized by reactions of the corresponding bis(imino)pyridyl ligands with $ZnCl_2$ in CH_2Cl_2 at room temperature (**Zn1**). A mixture of $ZnCl_2$ (53 mg, 0.39 mmol), $\mathbf{L^2}$ (187 mg, 0.39 mmol), CH_2Cl_2 (35 mL), pyridine-2,6-dicarboxylic acid (42.3 mg, 0.1 mmol) and distilled water (2 mL) was prepared. After the mixture had been stirred for 12 h, it was slowly cooled to room temperature and recrystallized twice with $V_{CH_3CN:CH_2Cl_2} = 2:1$. Well-shaped, light-yellow single crystals of complex **Zn1** (183 mg) suitable for X-ray four-circle diffraction analysis were obtained (yield *ca.* 76%, based on Zn).

Cd1 ($C_{33}H_{43}N_3CdCl_2$). $CdCl_2{\cdot}6H_2O$ (90 mg, 0.39 mmol) and $\mathbf{L^2}$ ligand (124 mg, 0.39 mmol) were stirred for 12 h in a reaction with a stoichiometric amount of the corresponding bis(imino)pyridyl ligands in 40 mL dichloromethane solution at room temperature. **Cd1** was obtained as yellowish crystals in good yield (yield *ca.* 76%, 177 mg).

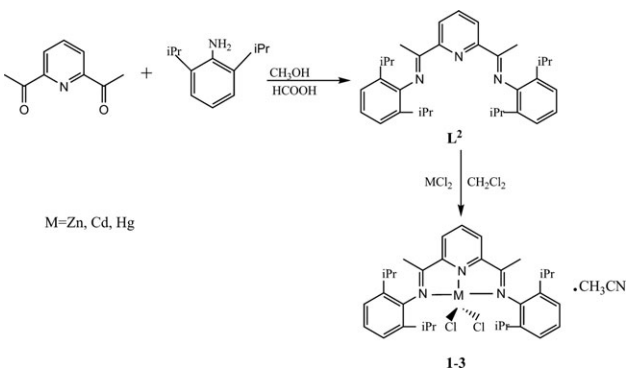

Scheme 1 Synthesis process of transition metal complexes.

Hg1 ($C_{33}H_{43}N_3HgCl_2$). A mixture of $\mathbf{L^2}$ (113 mg, 0.36 mmol) and $HgCl_2$ (98 mg, 0.36 mmol) in CH_3CN (20 mL) was stirred under nitrogen at room temperature for 12 h. Evaporation of the solvent gave the crude product as a yellowish powder. Pure product **Hg1** was obtained in 78% yield (179 mg) by recrystallization from CH_3CN–CH_2Cl_2 (2 : 1).

Photoelectrochemical measurements

The sample was sandwiched between two FTO glass electrodes. Optically transparent electrodes were made from an F-doped SnO_2-coated glass plate (FTO, 90% transmittance in the visible, 15 Ω^{-1} per square) purchased from Geao Equipment Company, Wu Han. The sensitizations were chosen: N719 (*cis*-bis(isothiocyanato)bis(2,2-bipyridyl-4,4-dicarboxylato)-ruthenium(II) bis-tetrabutylammonium or $RuL_2(NCS)_2$: 2 TBA (L = 2,2-bipyridyl-4,4-dicarboxylic acid, TBA = tetrabutylammonium, Solaronix Company, Switzerland) at a concentration of 3×10^{-4} M in absolute ethanol solution, and the co-sensitization dye of the three transition metal complexes in the form of single crystals were prepared in the same way. The electrolyte used in this work was 0.5 M LiI + 0.05 M I_2 + 0.1 M *tert*-butyl pyridine in a 1 : 1 (volume ratio) of acetonitrile–propylene carbonate. The films were stained by immersing them in 3×10^{-4} M absolute ethanol solution of **M1** and N719 for 2 and 12 h, respectively. Photovoltaic performance was measured by using a mask with an aperture area of 0.2 cm^2; the irradiance of sunlight was set at 100 mW cm^{-2}.

Based on a J–V curve, the fill factor (FF) is defined as: $FF = (J_{max} \times V_{max})/(J_{sc} \times V_{oc})$, where J_{max} and V_{max} are the photocurrent density and photovoltage for maximum power output (J_{sc} and V_{oc} are the short-circuit photocurrent density and open-circuit photovoltage, respectively), $\eta = (FF \times J_{sc} \times V_{oc})/P_{in}$ the overall energy conversion efficiency (η is defined as where P_{in} is the power of the incident light).

The EIS of cell measurements were taken at a working electrode potential of 550 mV over a frequency range of 0.1–100 000 Hz. Potential values are referred to with respect to a saturated calomel reference electrode (SCE). Glassy carbon and platinum electrodes were used as the working electrodes and a platinum wire was employed as the counterelectrode. A solution of 0.1 M tetrabutylammonium hexafluorophosphate ($TBAPF_6$, Fluka, electrochemical grade) in CH_2Cl_2 (Aldrich, anhydrous, 99.8%) were used as the supporting electrolyte. A mixed solvent system was employed to prevent adsorption on the electrode. Analyte concentrations of typically 1 mM were used.

Results and discussion

Photoelectrochemical measurements

Fig. 1 presents the performance of the DSSCs in terms of J_{sc} and V_{oc} in the transition metal complexes. The transition metal complex was assembled onto a nanocrystalline TiO_2 film to prepare a complex/N719 co-sensitized photoelectrode for DSSC applications. The results in Table 1 indicate that the

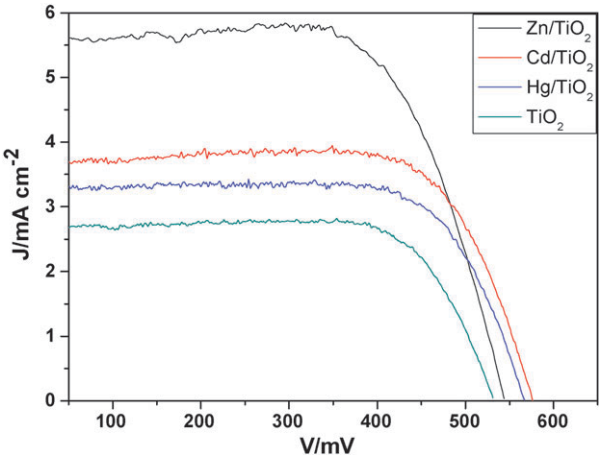

Fig. 1 *J–V* (current density–voltage) curves for the sunlight-illuminated DSSCs with different organometallic ligand complexes.

cell performance in co-sensitizer DSSCs with a mixture of transition metal complex and N719 are improved with fewer protons in elements. As shown in Table 1, the TiO_2/**Zn1**/N719 composite photoelectrode is selected as an example. The photochemical performance results indicate that the co-sensitized solar cell based on a TiO_2/**Zn1**/N719 electrode yielded a remarkably high photocurrent density (J_{sc}) of 5.47 mA cm^{-2} under standard global AM 1.5 solar irradiation conditions. The cell showed an open circuit voltage (V_{oc}) of 576 mV and an energy conversion efficiency of 4.55%, which were relatively higher than those for DSSCs using single organic sensitizers. In this way, the cell efficiency was improved by more than 2%.

Table 1 indicates that the photochemical performance of the co-sensitized photoelectrode has been increased with fewer protons in the transition metal complexes. The results also suggest that co-sensitized TiO_2 can be constructed with a higher UV-visible light activity over DSSCs containing an individual dye (see Table 1 for single dyes). This result suggests that the arrangement of the dyes on the TiO_2 film by, for example, aggregation and ordering of the chromophores, clearly influences the performance of the solar cell. The use of dyes with efficient light-harvesting properties at low energies and negligible intermolecular interactions is important for the development of efficient multidye solar cells. With increasing protons in atoms, the photoelectrons are extinguished, which is of no benefit for the movement of photoelectrons in TiO_2; therefore, the photochemical performance of the composite photoelectrode decreases. In a word, the photochemical performance of the composite co-sensitized TiO_2 photoelectrodes was increased compared to single raw TiO_2.

Table 1 Contrast of *J–V* performance between TiO_2/**M1**/N719 and raw TiO_2 photoelectrodes

Photoelectrode	V_{oc}/mV	J_{sc}/mA cm^{-2}	FF	η (%)
Raw TiO_2	544	2.66	0.76	2.21
Zn1/TiO_2	576	5.47	0.72	4.55
Cd1/TiO_2	567	3.69	0.75	3.14
Hg1/TiO_2	531	3.26	0.72	2.51

Cyclic voltammetric measurements

In order to explore the electrochemical behaviors of the title compounds, we carried out cyclic voltammetric measurements. Fig. 2 displays the cyclic voltammogram for 1.0 mM **M1** in CH_2Cl_2 containing 0.1 M $TBAPF_6$ solutions with scan rate of 100 mV s^{-1} at room temperature.

Fig. 2 shows that all the isopolyanions underwent a one-step two-electron transition metal reduction process (eqn (1)) according to the formula $E_{1/2} = |E_{pa} + E_{pc}|/2$, $E_{1/2} = 1.52 - (2.303\ RT/nF)$ (mV)[18] [n denotes the electrons that transferred].

$$C_{33}H_{43}N_3M(II)Cl_2 + 2e^- \rightleftharpoons C_{33}H_{43}N_3M(0)Cl_2 \qquad (1)$$

Compound **1** presented a similar electrochemical behavior to that of complexes of **2** and **3** in aqueous solution, implying that the polymeric structures of the compounds are nearly identical. However, the redox peak potential separations further increase and the peak positions are shifted to the positive potential direction with decreasing protons, implying that the reduction of isopolyanions is accompanied by protonation to maintain charge neutrality. Table 2 lists the peak potentials of cyclic voltammograms for the transition metal complexes.

Electrochemical impedance spectroscopy (EIS)

EIS is a powerful method of characterizing many of the electrical properties of materials and their interfaces with electronically conducting electrodes. It may be used to investigate the charge carrier dynamics in the bulk or interfacial regions of any kind of solid or liquid material, including ionic, semiconducting, mixed electronic–ionic conductors and even insulators (dielectrics).[19,20]

The first arc in the high frequency range of the Nyquist plot is assigned to the electron transfer process at the electrolyte/counterelectrode (CE) interface. This feature arises from an increase in the electron transport resistance of the mesoscopic TiO_2 film due to a decrease of the electron concentration. The electron transport process and charge recombination dominate the impedance spectra in the middle frequency range (from 100 to 1000 Hz). The increase of the radius of the semicircle in the Nyquist plot indicates a reduction in the

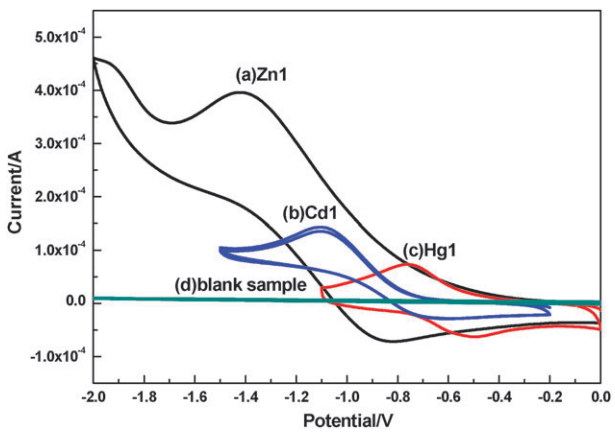

Fig. 2 Cyclic voltammograms of 1.0 mM **M1** and a blank sample in CH_2Cl_2 containing 0.1 M $TBAPF_6$ solutions with scan rate of 100 mV s^{-1}.

Table 2 Peak potentials of cyclic voltammograms for **Zn1**, **Cd1** and **Hg1**

Complex	Epc/V	Epa/V	ΔEp/V
Zn1	−1.41	−0.85	0.56
Cd1	−1.09	−0.70	0.39
Hg1	−0.75	−0.50	0.25

interfacial charge recombination rate due to a decrease in the conduction band electron concentration. The Warburg diffusion impedance for hole transport in electrolytes can be observed at low frequencies (less than 1 Hz). In accordance with Fig. 3, the impedance of the composite photoelectrode is increased with increasing protons in atoms, which is of no benefit for the photochemical performance of DSSC.

A physical model has been proposed to understand the complex charge-transfer processes that take place in DSSCs.[21,22] As shown in Fig. 4, R_s represents series resistance consisting of Ohmic components. R_1 and R_2 are resistance components forming a parallel circuit with constant phase elements (CPE). Furthermore, C is roughly equal to the differential electric capacitances because there is almost no depression of the semicircles. Under light irradiation conditions, R_1 estimated from semicircle 2 was remarkably larger with decreasing protons. Hence, we conclude that lower frequency semicircle 2 originated from TiO_2/**M1** composite photoelectrodes as an n-type inorganic semiconductor.

Surface photovoltage spectrum analysis

The surface photovoltage spectrum (SPS) method is commonly applied to TiO_2 for DSSCs, which is a well-established contactless technique for surface state distribution.[23,24] As shown in Fig. 5, the SPS analysis is described for samples with d^{10} transition metal co-sensitization of composite TiO_2 photoelectrodes. It shows one typical characteristic response band close to 350 nm that originates from the band–band electron transition of TiO_2. However, for composite TiO_2 photoelectrodes, a new SPS signal from 500 to 600 nm is observed, assigned to the band–band electron transition of the d^{10} metal co-function with TiO_2 in the composite photoelectrode. The results also show that the composite TiO_2 is beneficial for visible light response range broadening from 400 to 500 nm and continuous after co-sensitization in DSSC photoelectrodes.

The relationship between crystal structures and electrochemical properties

From the synthetic chemists' point of view, the geometric and electronic structure of the sensitizer also play an important role. When all these factors are taken into account, it should be possible to design more sophisticated and appropriate dye structures that satisfy the needs of DSSC technology.

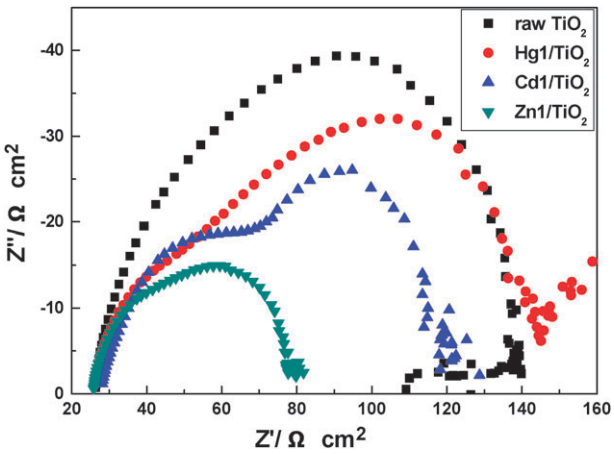

Fig. 3 Nyquist plots of the transition metal complex/N719 co-sensitized DSSC in standard global AM 1.5 solar irradiation.

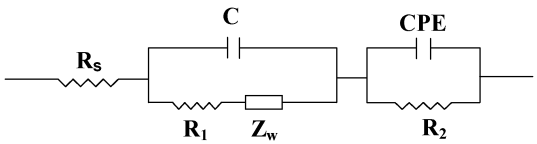

Fig. 4 Equivalent circuit used to model this system, representing interfaces in composite solar cells composed of FTO|TiO_2/**M1**-dye|I_3^-/I^-||Pt|FTO (component explanation: R_s = series resistance, R_1, R_2 = charge-transfer resistance, C = double layer capacitance, CPE = symbol for the constant phase element and Z_w = Warburg impedance).

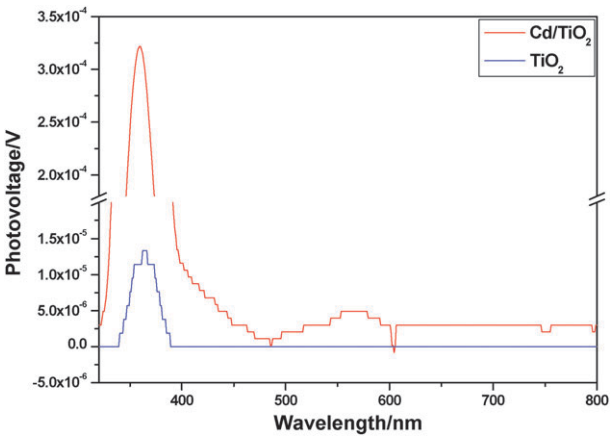

Fig. 5 SPS of transition metal complex co-sensitized TiO_2 and raw TiO_2.

Table 3 Parameters obtained by fitting the impedance spectra of composite solar cells using the equivalent circuit in Fig. 4

DSSC samples	R_s/Ω	C/F	R_1/Ω	Z_w (Y_{O1}/S)	R_2/Ω	CPE (Y_{O2}/Fs^{n-1})	n
Raw TiO_2	53.51	2.51E-5	54.97	2.119E-8	25.85	1.854E-5	0.803
Zn1	38.011	6.339E-6	46.28	3.915E-2	25.62	2.062E-4	0.664
Cd1	39.59	1.533E-4	51.16	1.462E-1	27.36	5.121E-5	0.704
Hg1	41.4	8.861E-5	78.61	5.035E-2	35.21	1.47E-4	0.554

Single-crystal structural analyses revealed that compounds **1**, **2** and **3** are isostructural[25,26] (see the ESI†). The complex possesses a structure with approximate C_s symmetry about a plane containing the cadmium atom, two chlorine atoms and the pyridine nitrogen atom. For both molecules, the central cadmium atom is coordinated to five atoms, and the geometry about the cadmium/zinc/mercury atoms is distorted trigonal-bipyramidal, crystallizing in the polar space group $P\bar{1}$; the unit cell dimensions, volumes, related bond distances and angles are only slightly changed.

As shown in Fig. 6, the equatorial plane is defined by the N(2)(pyridine), Cl(1) and Cl(2) atoms, with the N(1) and N(3)(imino) atoms in the axial positions. The molecular structure of the complex is shown below, and selected bond lengths and angles are presented in Tables S2–S4.† There are two independent planes of phenyl rings, oriented approximately orthogonally to the plane of the three coordinated nitrogen atoms. The dihedral angles between the two phenyl rings decrease with the proton numbers; **Zn1** is chosen for explanation. The angles between two molecules in the equatorial plane range around 70°, and the axial Zn–N(imino) bonds subtend an angle of 139°, which decreases from Zn to Hg.

In the coordination polyhedron around Zn, the N1, N2 and N3 atoms form two phenyl rings. This is one of the common coordination geometries for complexes with a coordination number of five. The crystal lattice distances are divided into two different types presented in the coordination sphere of the transition metal (see Table 4). The data show bond lengths Hg–N > Cd–N > Zn–N, Cd–Cl > Hg–Cl > Zn–Cl, indicating that the Zn–N and Zn–Cl bonds are more stable than the others. The Zn atom deviates by 0.56 Å away from the coordination plane in a single molecule, while the mean deviation of the Zn atom from the equatorial plane in a single molecule is only 0.013 Å; they all increase with proton numbers. Fig. 7 shows the packing diagram of **Zn1** along the *c* axis. Hydrogen bonds are indicated by dashed lines. From the data shown in Table 4, the hydrogen bond lengths decreased with increasing proton number. Corresponding to their electrochemical properties, it can be concluded that the electron-donating ability is in favor of a stable single molecule structure with copious space between molecules. Therefore, it is common that the decrease of bond lengths and deviation distances are advantageous to electrochemical properties, while the enlargement of dihedral angles leads to superior cell performance according to Fig. 8.

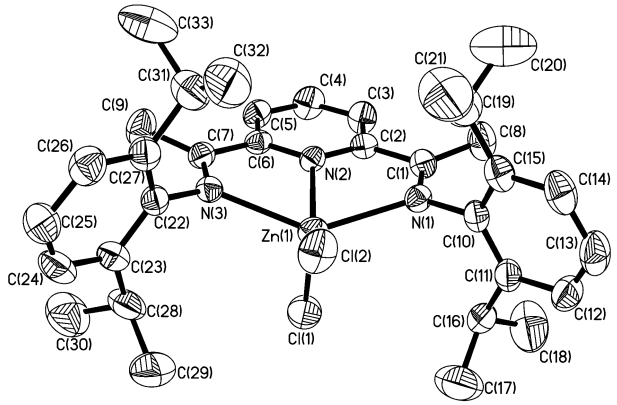

Fig. 6 The asymmetric unit of **Zn1**.

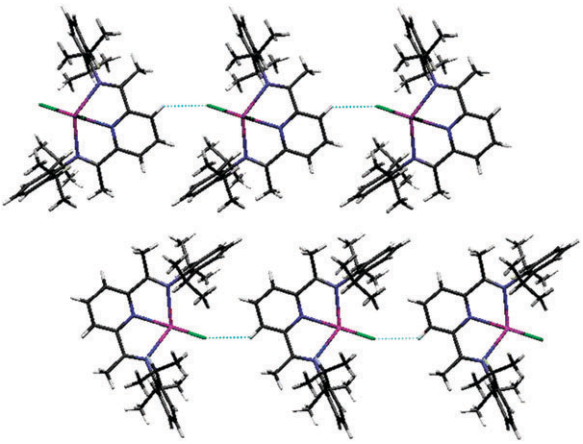

Fig. 7 Packing diagram of the complex **Zn1** along the *c* axis. Hydrogen bonds are indicated by dashed lines.

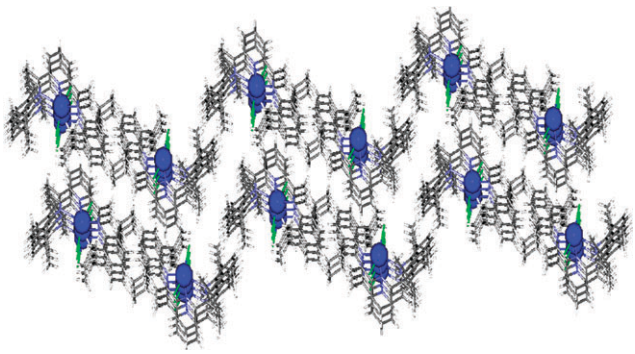

Fig. 8 The 3-D structure of complex **Zn1** with π–π stacking interaction.

Conclusions

In this paper, we have presented three d^{10} metal coordination complexes with pyridine-type ligands through systematic basic research that represent mosaic pieces for future research and

Table 4 The contrast in bond lengths and angles of the molecular structures of the transition metal complexes

	Bond lengths of **M**–N/Å	Bond lengths of **M**–Cl/Å	Hydrogen bond lengths/Å	Distance of **M** deviated away from the coordination plane/Å	Deviation distance of **M** from the equatorial plane/Å	Dihedral angles of N–**M**–N (°)	Dihedral angles between phenyl rings and the coordination plane (°)
Zn1	2.313	2.251	2.887	0.560	0.013	72.88(8)	139.88(8)
Cd1	2.480	2.411	2.744	0.652	0.027	68.29(17)	131.99(16)
Hg1	2.513	2.364	2.746	0.740	0.032	65.4(2)	126.6(2)

development. DSSC technology undoubtedly has an exciting future and there remain vast opportunities to ameliorate performance. Therefore, the development of a conceptually new design for constructing metal coordination dyes is an important and urgent challenge. We also believe that the versatility of the synthetic design concept will continue to inspire research on this topic.

Acknowledgements

This work was supported by the National Science Foundation of China (Grant no. 20971031, 20671025 and 20771030) and the China Postdoctoral Science Foundation funded project (no. 65204).

References

1 S. M. Yang, H. Z. Kou, H. J. Wang, K. Cheng and J. C. Wang, *New J. Chem.*, 2010, **34**, 313.
2 C. Strümpel, M. McCann, G. Beaucarne, V. Arkhipov, A. Slaoui, V. Švrček, C. del Cañizo and I. Tobias, *Sol. Energy Mater. Sol. Cells*, 2007, **91**, 238.
3 B. O'Regan and M. Grätzel, *Nature*, 1991, **353**, 737.
4 M. K. Nazeeruddin, A. Kay, I. Rodicio, R. Humphrybaker, E. Muller, P. Liska, N. Vlachopoulos and M. Grätzel, *J. Am. Chem. Soc.*, 1993, **115**, 6382.
5 P. V. Kamat, *J. Phys. Chem. C*, 2008, **112**, 18737.
6 A. Kongkanand, K. Tvrdy, K. Takechi, M. Kuno and P. V. Kamat, *J. Am. Chem. Soc.*, 2008, **130**, 4007.
7 T. Lopez-Luke, A. Wolcott, L. P. Xu, S. Chen, Z. Wen, J. H. Li, E. De La Rosa and J. Z. Zhang, *J. Phys. Chem. C*, 2008, **112**, 1282.
8 T. Funaki, M. Yanagida, N. Onozawa-Komatsuzaki, K. Kasuga, Y. Kawanishi, M. Kurashige, K. Sayama and H. Sugihara, *Inorg. Chem. Commun.*, 2009, **12**, 842.
9 Y. L. Lee and Y. S. Lo, *Adv. Funct. Mater.*, 2009, **19**, 604.
10 W. Lee, S. H. Kang, S. K. Min, Y. E. Sung and S. H. Han, *Electrochem. Commun.*, 2008, **10**, 1579.
11 W. Y. Wong, *J. Organomet. Chem.*, 2009, **694**, 2644.
12 W. Wu, F. Meng, J. Li, X. Teng and J. Hua, *Synth. Met.*, 2009, **159**, 1028.
13 Y. S. Chen, Z. H. Zeng, C. Li, W. B. Wang, X. S. Wang and B. W. Zhang, *New J. Chem.*, 2005, **29**, 773.
14 A. Ehret, L. Stuhl and M. T. Spitler, *J. Phys. Chem. B*, 2001, **105**, 9960.
15 Y. S. Chen, Z. H. Zeng, C. Li, W. Wang, X. S. Wang and B. W. Zhang, *New J. Chem.*, 2005, **29**, 773.
16 M. Guo, P. Diao, Y. J. Ren, F. S. Meng, H. Tian and S. M. Cai, *Sol. Energy Mater. Sol. Cells*, 2005, **88**, 23.
17 J. H. Yum, S. R. Jang, P. Walter, T. Geiger, F. Nüesch, S. Kim, J. Ko, M. Grätzel and M. K. Nazeeruddin, *Chem. Commun.*, 2007, 4680.
18 R. Hage, A. H. J. Dijkhuis, J. G. Haasnoot, R. Prins, J. Reedijk, B. E. Buchanan and J. G. Vos, *Inorg. Chem.*, 1988, **27**, 2185.
19 C. Longo, J. Freitas and M. A. De Paoli, *J. Photochem. Photobiol., A*, 2003, **159**, 33.
20 J. G. Chen, C. Y. Chen, S. J. Wu, J. Y. Li, C. G. Wu and K. C. Ho, *Sol. Energy Mater. Sol. Cells*, 2008, **92**, 1723.
21 K. Mukherjee, T. H. Teng, R. Jose and S. Ramakrishna, *Appl. Phys. Lett.*, 2009, **95**, 012101.
22 J. E. Trancik, S. C. Barton and J. Hone, *Nano Lett.*, 2008, **8**, 982.
23 H. Irie, Y. Watanabe and K. Hashimoto, *J. Phys. Chem. B*, 2003, **107**, 5483.
24 L. Q. Jing, X. J. Sun, J. Shang, W. M. Cai, Z. L. Xu, Y. G. Du and H. G. Fu, *Sol. Energy Mater. Sol. Cells*, 2003, **79**, 133.
25 R. Fan, Y. Yang, Y. Yin, W. Hasi and Y. Mu, *Inorg. Chem.*, 2009, **48**, 6034.
26 R. Fan, Y. Zhang, Y. Yin, Q. Su, Y. Yang and W. Hasi, *Synth. Met.*, 2009, **159**, 1106.

